Pressure Drop Across Aortic Valve with Aortic Stenosis Using 3D Model and Pulsatile Flow

Madeline Fabela with Dr. Erica Kemmerling
Department of Mechanical Engineering, Bray Laboratory 101, Tufts University, 504 Boston Ave, Medford, MA 02155, USA

Abstract

Stenosis of the aortic valve or aortic stenosis can be caused by calcium buildup that leads to a reduction in the free area of the valve which restrains the flow of blood to the aorta. A 3D-printed model of a patient's stenosis was created using CT scan data provided by Tufts Medical Center. The 3D-printed model was used to physically measure the pressure gradient produced when tested with steady and pulsatile flow conditions. Steady flow was used to validate the 3D-printed model as a representation of a patient's aortic valve. Dynamic similarity allowed for water to be used instead of blood. Matching Reynolds and Womersley numbers for blood and water were used to find the water flow rates and frequency that were necessary to match hemodynamic conditions. The resulting water flow rate for steady conditions in the experimental setup was about 712 mL/min. There were 20 trials done for the steady flow simulation with a resulting average blood pressure of 484.21 mmHg. This value is above the permissible range for patients with aortic stenosis. It was determined that the results confirmed that with more accurate flow conditions, the 3D-printed model could prove to be an accurate replica of a patient's aortic valve. Therefore, the study was continued with pulsatile flow. The flow changed over time based on hemodynamic conditions but was limited by the operational restrictions of the pump used. Blood flow through the aorta was plotted versus time and used as a source for matching water flow rates every 0.2 seconds to blood flow rates. Initially, the 5 flow rates were extracted from the data but due to the backflow of blood and other limitations, there were only 3 real flow points that were tested. The final five water flow rates after conversions and calibrations were done were 2796.13 mL/min, 0 mL/min, 201.3 mL/min, 34.77 mL/min, and 0 mL/min. These took a total of 2.83 seconds to loop through the 3D-printed model, which matched the frequency of blood flow. For the pulsatile flow simulation, there were 4 trials total each with 9 cycles of the five flows. The average pressure gradients for blood that corresponded to the three main flows were 304.19 mmHg, 34.08 mmHg, and 0 mmHg. These results are within real pressure gradients experienced by patients with severe aortic stenosis, confirming that 3D-printed models of patients' aortas can provide health professionals with patient-specific blood pressure gradients.

1. Motivation and Background

1.1 Aortic Stenosis Overview

Aortic stenosis is one of the most prominent heart diseases in the developed world (Grimard et al., 2016). Therefore, there is a great need for patient-specific data to help diagnose and treat this disease better. It is widely caused by calcium deposits that build up and solidify,

causing the aortic valve to become restricted in movement (Grimard et al., 2016). Some patients have aortic stenosis from birth, however, this study will focus on patients with aortic stenosis from calcification. Aortic stenosis affects people with both tricuspid and bicuspid aortic valves. Nevertheless, patients with a bicuspid valve are diagnosed with aortic stenosis sooner and more often than patients with tricuspid valves. While individuals with tricuspid valves generally receive a diagnosis in their 60s, 70s, and 80s, people with bicuspid valves often develop stenosis beginning in their 40s. Furthermore, bicuspid aortic valves are dominant in male patients. This leads to males being more likely to have aortic stenosis (Carabello & Paulus, 2009).

The heart's left ventricle is responsible for pumping blood out of the heart and into the aorta. The aortic valve serves as a gate that expands and contracts to either let blood flow to the aorta or to contain such flow (*Aortic Stenosis*, 2022). Figure 1 shows the position of the aorta, aortic valve, left ventricle, and where stenosis builds up in the heart. Calcification of the aortic valve hinders the outflow of blood from the left ventricle. This leads to there being significantly more strain on the muscles of the heart since the same amount of blood has to pass through a smaller open area which forces the heart's muscles to work harder. As a consequence, the left ventricle myocardium increases in size to counterbalance the effects of the obstruction (Grimard et al., 2016).

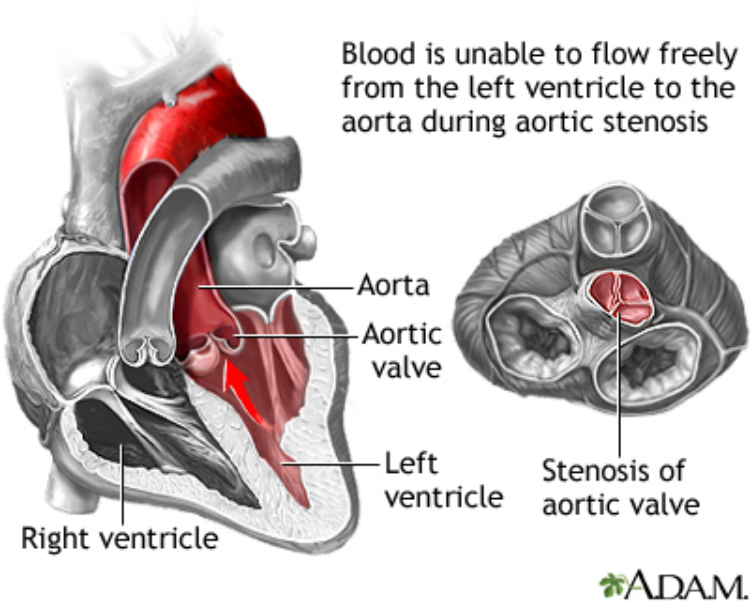

Figure 1 - Sectioned heart diagram highlighting body parts affected by aortic stenosis and a brief explanation of this condition (*Aortic Stenosis*, 2022)

1.2 Symptoms

One of the main causes of high mortality rates in people with aortic stenosis is the various symptoms. Unfortunately, once severe symptoms arise, the patient gains an increase in mortality rate close to 25% every year. Syncope, also referred to as fainting, is one such symptom; it arises when a patient does physical exercise (*Syncope (Fainting)*, 2022). The specifics of how syncope functions as a result of aortic stenosis are not known. Carabello and Paulus explain that syncope could be due to vascular resistance decreasing during exercise but flow staying nearly constant due to the obstruction keeping flow constrained, this by definition causes blood pressure to drop. Resistance of blood vessels can be found by dividing the pressure gradient by the amount of flow measured (Delong & Sharma, n.d.).There is also heart failure, angina, and atrial fibrillation. Heart failure happens when the heart becomes too weak to pump the blood supply the human body needs (*Heart Failure - Symptoms and Causes*, 2023). Connected to heart failure, atrial fibrillation is when the heartbeat becomes faster than usual and pumps abnormally (National

Library of Medicine, n.d.). This happens when the heart no longer exerts the force needed for the atria to contract and send blood to the right and left ventricles. This leads to less blood filling and getting through the atria. This symptom only happens in a relatively small amount of patients with aortic stenosis but can have unfortunate consequences. Lastly, angina is pain experienced in one's chest caused by the additional oxygen needed to make up for the increase in the size of the left ventricle myocardium (National Library of Medicine, n.d.). As mentioned previously, aortic stenosis can impose strain on the heart that over time weakens it; this all leads to the atrium not having the proper supply of blood. This results in a decrease in the oxygen level supplied to the left ventricle. The reduction of oxygen combined with an increased need for oxygen results in the patient experiencing angina (Grimard et al., 2016). All of these symptoms cause the heart to deteriorate and eventually fail in its primary functions. This can lead to a reduced quality of life or even fatal results. Therefore, it is important to have an accurate procedure for collecting pressure gradient data to help with the diagnosis of aortic stenosis.

1.3 Diagnosis and Treatment

Diagnosis can be difficult when it comes to aortic stenosis. Initially, aortic stenosis can be noticed because of irregular heart murmurs. Depending on how severe the stenosis is, heart murmurs can happen at varying times, become more audible, and disrupt the trajectory of carotid upstrokes. For patients with moderate stenosis, murmurs happen in the initial part of systole. The heartbeat is made up of two phases, systole is the second phase in which ventricles contract and blood is pushed out through the pulmonary and aortic valves (The Texas Heart Institute, n.d.). As the severity of stenosis increases, the occurrence of murmurs happens later during systole. More severe stenosis also causes louder murmurs and carotid upstrokes to peak later during systole (Carabello & Paulus, 2009). Though murmurs are a sign of heart disease, they alone are not enough to diagnose a patient with aortic stenosis. For a more secure diagnosis, imaging tools are used to visualize and measure the area of the aortic valve that is still free of obstruction, these include echocardiograms, cardiac computed tomography (CT), and magnetic resonance imaging (MRI). Echocardiograms can record visuals of one's aortic valve. These videos help health professionals diagnose varying heart conditions without the use of radiation or harmful substances. Similar to echocardiograms, CT scans are used to help cardiologists see obstructions inside one's heart through the use of X-rays. 3D views are possible with CT scans but these are in image form rather than video. Lastly, an MRI can provide doctors with precise images of one's heart and its condition. An MRI scans the heart with the use of radio waves and magnets (*Cardiac Imaging: Types, Uses and Procedure Details*, 2022). These methods of cardiac imaging are helpful in the diagnosis of aortic stenosis since the free area of the aortic valve is an indicator of the severity of this condition.

The maximum velocity of blood through the aorta and into the left ventricle as well as the pressure gradient across the aorta are also indicators of how severe the obstruction is. If the maximum velocity of blood is measured to be greater than 4 m/s or if the average pressure gradient is greater than 40 mm Hg, aortic stenosis can be classified as severe. Currently, the only

way to treat aortic stenosis is with a heart valve replacement. Nevertheless, the decision to recommend such treatment is based initially on the severity of the obstruction as well as whether the patient is asymptotic or symptomatic. Other factors are taken into account such as surgical risk, and how fast the obstruction is growing; if it is determined a patient should not undergo an aortic valve replacement, they are monitored closely to ensure conditions do not become worse (Grimard et al., 2016).

Because a significant amount of people who are diagnosed with aortic valve stenosis are older than 50, it can be complicated to recommend surgical procedures since they come with a lot of complications and risks. However, because a successful surgical valve replacement could increase a patient's chances of survival significantly, some doctors believe this is the best option for specific patients. Furthermore, there are cases of asymptomatic patients who experience symptoms suddenly and then die abruptly. Though this affects a very small part of individuals with aortic stenosis, it is reason enough to suggest heart valve replacement to an asymptotic patient (Carabello & Paulus, 2009). People who undergo successful surgery to replace the aortic valve can have a life expectancy of up to 10 years. For patients who may suffer complications during or after surgery due to medical conditions, age, or other causes, transcatheter aortic valve replacement can be a better option. Such surgical risks should be reviewed by cardiologists and cardiac surgeons. Every patient is unique and doctors need to accurately diagnose one's stenosis before deciding if they should undergo a procedure (Grimard et al., 2016). This is one of the main motivations for this study, as patient-specific 3D-printed models could be beneficial when deciding how severe one's obstruction is and how to best treat it based on one's pressure gradient.

2. Related Work

2.1 Related Work - Steady Flow

This study aims to simulate blood flow using a patient-specific 3D-printed model of their aortic stenosis to obtain the pressure gradient experienced across the aortic valve. Other studies also aim to model aortic stenosis to analyze its effects on one's body. Ghalichi et. al. were able to determine the indicative Reynolds number for transitional or turbulent flow by applying the Wilcox low-Re turbulence model to flow simulations of stenoses of varying areas (Ghalichi et al., 1998). There is also research that has focused on analyzing or modeling blood flow in hearts with aortic stenosis to help diagnose aortic stenosis. One study by the Journal of the American College of Cardiology aimed to see the correlation between blood flow rate and functional valve area. The study found that measuring the open area in the aortic valve is not an accurate metric for diagnosis with low blood flow rates (Namasivayam et al., 2020). Hatle et al focused on using blood flow velocity to determine the severity of the stenosis. It was concluded that maximal velocity can be used to determine the severity of stenosis in patients who are under 50 years old (Hatle et al., 1980). Hayek et. al. studied systolic blood pressure to determine if it is related to the diagnosis of aortic stenosis and found that it can lead to an underevaluation of aortic stenosis severity (Hayek et al., 2020). A study by the Journal of the American Society of

Echocardiography focused on modeling blood flow using computational fluid dynamics. Though the results of the study overestimated pressure drops for low-flow simulations, it showed great promise for future computations of the pressure gradient (Hoeijmakers et al., 2019). All of these studies explore the importance of understanding flow properties in aortic stenosis and give useful contributions to the future of aortic stenosis models. Nevertheless, these focus on steady flow which is not representative of how the blood flows through the aortic valve.

2.2 Related Work - Pulsatile Flow

Other studies have incorporated pulsatile flow which mimics hemodynamics more accurately than steady flow. Voelker et al were able to develop a model that included different sizes and shapes of stenoses and measured pressure recovery values to juxtapose them with values derived from fluid dynamic calculations (Voelker et al., 1992). A different study used nozzles to represent the reduction in the open area caused by stenosis combined with both, pulsatile and steady flow to obtain velocity measurements (Clark, 1976). Another study by Voelker et al investigated how valvular resistance, stroke work loss, and Gorlin valve area can help diagnose aortic stenosis; this study found that valvular resistance is an appropriate indicator of the severity of aortic stenosis (Voelker et al., 1995). Keshavarz-Motamed and Kadem created a simplified model of the flow conditions in the aorta with coarctation as well as an aortic valve with stenosis. Their results indicated that aortic stenosis and coarctation together have a significant effect on wall shear stress and pressure loss (Keshavarz-Motamed & Kadem, 2011). Furthermore, Maragiannis et al were able to create a 3D-printed model of a patient's stenosis which proved to be a good replica of valves with severe stenosis (Maragiannis et al., 2014). Lastly, Padmanabhan demonstrated that a mathematical model of aortic stenosis can be an adequate representation of hemodynamic conditions of aortic flow (Padmanabhan, 1980). These studies have all proven that it is possible to use varying models of aortic stenosis to output accurate results such as shear stress, pressure, or velocity values. Nevertheless, this study uses patient-specific data to create a 3D-printed model of one's stenosis rather than generalized models. This is important because each patient has unique needs for their specific stenosis. Therefore, a singular model cannot be used for analyzing to conditions of several patients which is why there is a need for the procedure used in this study.

This study uses a 3D patient-specific model of an aortic valve with severe aortic stenosis to measure pressure drop across the aortic valve. Such pressure drop values will allow health professionals to have a better method of diagnosing aortic stenosis. Calibrations on various pieces of equipment, dynamic similarity, as well as steady flow trials and pulsatile flow trials allowed for this study to be validated in terms of accuracy when measuring pressure gradients.

3. Overall Methods

3.1 Overview of Setup

This study used a 3D-printed model of a patient's aortic valve. The model was created using CT scans of an anonymous patient whom cardiologists at Tufts Medical Center diagnosed

with aortic stenosis. The initial Computer Aided Designed model was created using a segmentation technique that separated the open area of the aortic valve from the calcification. Several images of different layers of the aorta were segmented and compiled to create a final 3D-printed model.

For the setup, various water pumps were utilized to have water flow through the 3D model mimic the real flow of blood. Both, steady and pulsatile flows were tested. Steady flow trials needed a pump that was able to remain at a singular flow rate setting. When implementing pulsatile flow, a different pump with remote control was operated. The pump was activated and controlled by a LabView program and a NI 9263 analog output block. The pressure transducer was attached to two openings on the 3D model to measure pressure drop across the modeled aortic valve. Varying depending on the value of the pressure gradient produced, the pressure transducer sent a voltage signal out. Lastly, a multimeter read such signals and they were converted to their corresponding pressure gradient values in mmHg.

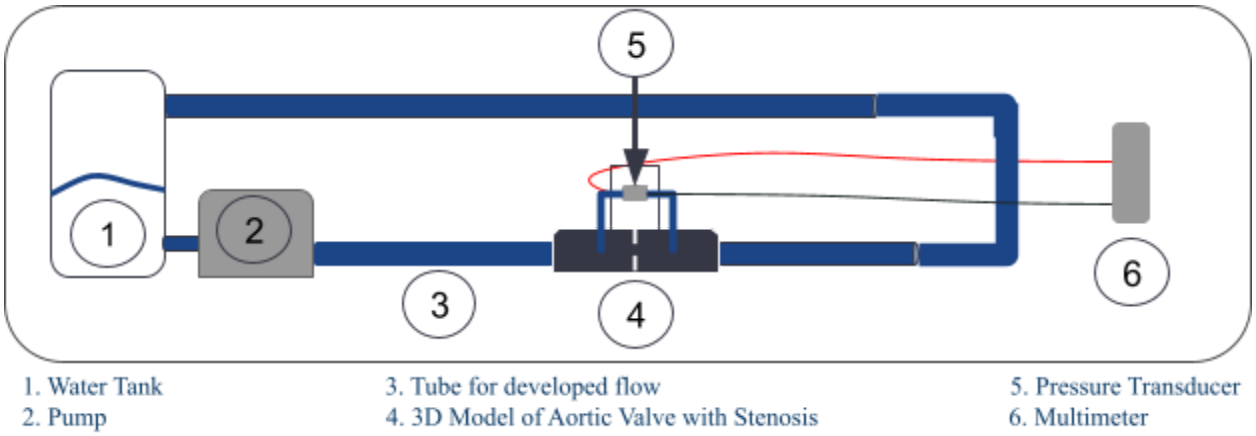

Figure 2 - Diagram of setup for recirculating flow trials

3.2 Setting and Participants

All of the trials took place in the Tufts Body Flow Laboratory in the Bray Lab building of Tufts University. The 3D-printed model was produced using the Stratasys F120 located in the 3D Printing Laboratory of the Bray Lab building as well. CT scans from a patient's occlusion were acquired from Tufts Medical School. The patient's identity was kept confidential which allowed this study to be exempt from IRB approval.

3.3 3D Printed Model and Connections

Calcium build-up is visible in images from CT scans and can be differentiated from bone and other materials. Therefore, CT scans segmented manually were used to create an accurate CAD model of the stenosed valve. Due to the complicated process of interpreting CT scan images, it was assumed that a certain pigment of gray was present in all images and represented tissue. It was also assumed that the images had a resolution adequate to capture the shape of the

wall accurately. Multiple layers of the occlusion's geometry were processed to model the final 3D shape of the occlusion.

\

Figure 3 - Display of the occlusion in the 3D-printed model

Once modeled, the 3D profile of the occlusion was extracted from the inside of a cylindrical tube. A fillet was added at the beginning of the stenoses geometry to prevent minor loss. Figure 3 shows the 3D-printed model once finished, acetone was used to smooth the surface lines. The white region displayed on the inside of the printed model is the free area of the aortic valve during diastole. The cylindrical opening on both ends has the same diameter as the tubing used to develop the flow and eventually connects from the pump to the 3D printed model and back to a water reservoir.

Additionally, the tubing attached to both ends of the 3D printed model had a diameter of 0.02 m which is consistent with the diameter of an aorta. Tube 1 was attached to the pump through smaller tubes and tube adapters. Tube 2 went back to a water reservoir that supplied water to the pump. The length of Tube 1 was 1.6 m which was determined by equating the Reynolds number of water and blood to agree with dynamic similarity; the details of this will be explained in a future section. The procedure for dynamic similarity that allowed for water to be used instead of blood will be mentioned in a future section as well. A pressure transducer was attached to two openings on the top surface of the 3D-printed model with the use of adapters to measure the difference in pressure across the aortic valve. The setup can be seen in Figure 4.

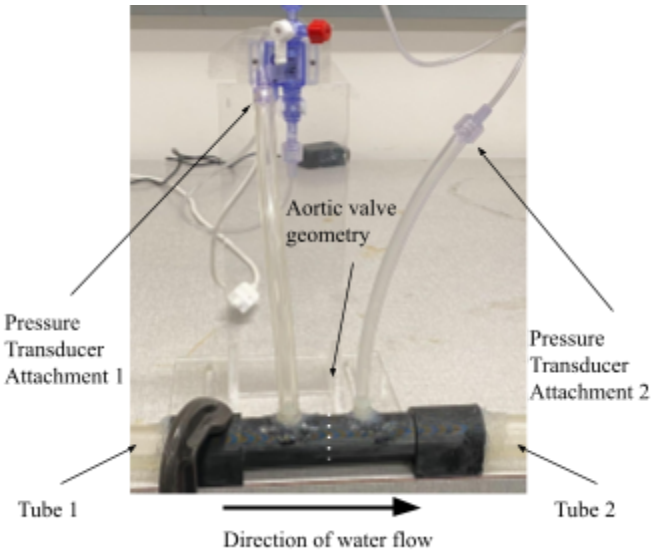

Figure 4 - Display of 3D printed model, pressure transducer, Tube 1, and Tube 2

3.4 Dynamic Similarity

Blood was not used in this study because it is biohazardous, as well as more expensive, prone to clogging, and harder to obtain when compared with water. The principle of dynamic similarity allowed for water to be used instead. To do this, the Navier-Stokes equations and boundary conditions of the experiment need to be nondimensionalized. Boundary conditions can be nondimensionalized when multiplied by relevant scaling factors that have the same units. Once this is done, depending on what boundary conditions are used, unitless parameters result to be the only indicator that dynamic similarity depends on to hold. In this study, the Reynolds number was used to find water velocity. The Reynolds number of a flow is defined as the flow's inertia divided by its viscous forces. The higher the viscous forces, the lower the Reynolds number becomes for a specific flow, this entails a more laminar profile since it is harder to disrupt the flow. On the other hand, the higher the flow's inertia, the higher the Reynolds number and the higher the speed of the fluid which means the flow becomes more likely to experience turbulence. Furthermore, the pressure recovery coefficient was used to find blood pressure, and the Womersley number was used to find the frequency of water during pulsatile flow trials following dynamic similarity. The Womersley number is the ratio of the flows' unsteady inertial forces over the viscous forces. The greater the Womersley number, the more likely it is to be more dominant unsteady effects in the flow.

3.5 Matching Reynolds Number

Initially, the Reynolds number of blood was found using a volumetric flow rate for blood of $8.33\frac{m^3}{s} * 10^{-5}$ based on a study done by Garcia et. al. in which aortic blood velocity was measured (2018).

$$Q_{blood} = 8.33\frac{m^3}{s} * 10^{-5}$$
$$\rho_{blood} = 1060\ \frac{kg}{m^3}$$
$$D_{aorta} = 0.02\ m$$
$$\mu_{blood} = 4 * 10^{-3} Pa * s$$

$$Re_{blood} = \frac{4Q_{blood}\rho_{blood}}{\pi D_{aorta}\mu_{blood}}$$
$$Re_{blood} = \frac{4*8.33\frac{m^3}{s}*10^{-5}*1060\frac{kg}{m^3}}{\pi*0.02m*4*10^{-3}Pa*s}$$
$$Re_{blood} = 1405.31$$

The Reynolds number of blood was used as a parameter to find the corresponding velocity of water for the steady flow trials. This velocity was then converted to a flow rate that the pump could produce. The following parameters and calculations were used:

$$\rho_{water} = 998.21\frac{kg}{m^3}$$
$$D_{aorta} = 0.02\ m$$
$$\mu_{water} = 1 * 10^{-3} Pa * s$$
$$Re = \frac{4\,Q\,\rho}{\pi\,D\,\mu} = \frac{4\,(\frac{1}{4}*\pi*D^2 u)\,\rho}{\pi\,D\,\mu} = \frac{u\,\rho\,D}{\mu}$$

$$u_{water} = \frac{\mu_{water}*1405.31}{\rho_{water} D_{aorta}}$$
$$u_{water} = \frac{1*10^{-3}Pa*s*1405.31}{998.21\frac{kg}{m^3}*0.02m}$$
$$u_{water} = 0.07\ m/s$$
$$Q_{water} = A * u_{water}$$
$$Q_{water} = (\pi * 0.01^2 m^2) * 0.07\ m/s$$
$$Q_{water} = 2.21 * 10^{-5} m^3/s$$
$$2.21 * 10^{-5}\frac{m^3}{s} * 60\frac{s}{min} * 1{,}000{,}000\frac{mL}{m^3} = 1328.89\ \frac{mL}{min}$$

$$Re_{blood} = Re_{water}$$
$$1405.31 = \frac{u_{water}\rho_{water}D_{aorta}}{\mu_{water}}$$

The Reynolds number of water was used to determine the entrance length needed for the flow to develop fully (Morini, n.d.).

$$0.05 * D_{aorta} * Re_{water} = Entrance\ Length \quad \textbf{(2)}$$
$$0.05 * 0.02\ m * 1405.06 = 1.405\ m$$

Aortic flow rate values were recorded and plotted as shown in Figure 5. Figure 5 is not entirely accurate because the negative flow rate caused by occasional backflow was set equal to 0. This was done because the pump was unable to make water flow opposite of the pumped direction. This should not affect the results because the crucial times in which the pressure gradient is the greatest are the two peaks. Moreover, five key flow rate values from Figure 5 were used to find the corresponding water flow rates the pump needed to output. Dynamic similarity allowed for the Reynolds number to be utilized to find the water flow rates from blood flow rates as follows:

$$Re = \frac{u_{blood}{}^{*}D}{v_{blood}} = \frac{u_{water}{}^{*}D}{v_{water}} \qquad v_{water} = 10^{-6}\frac{m^2}{s} \qquad v_{blood} = 4 * 10^{-6}\frac{m^2}{s} \qquad u_{water} = \frac{u_{blood}{}^{*}v_{water}}{v_{blood}}$$

$$u_{water} = \frac{u_{blood}}{4} \quad \textbf{(3)} \qquad\qquad Q_{water} = A * u_{water}$$

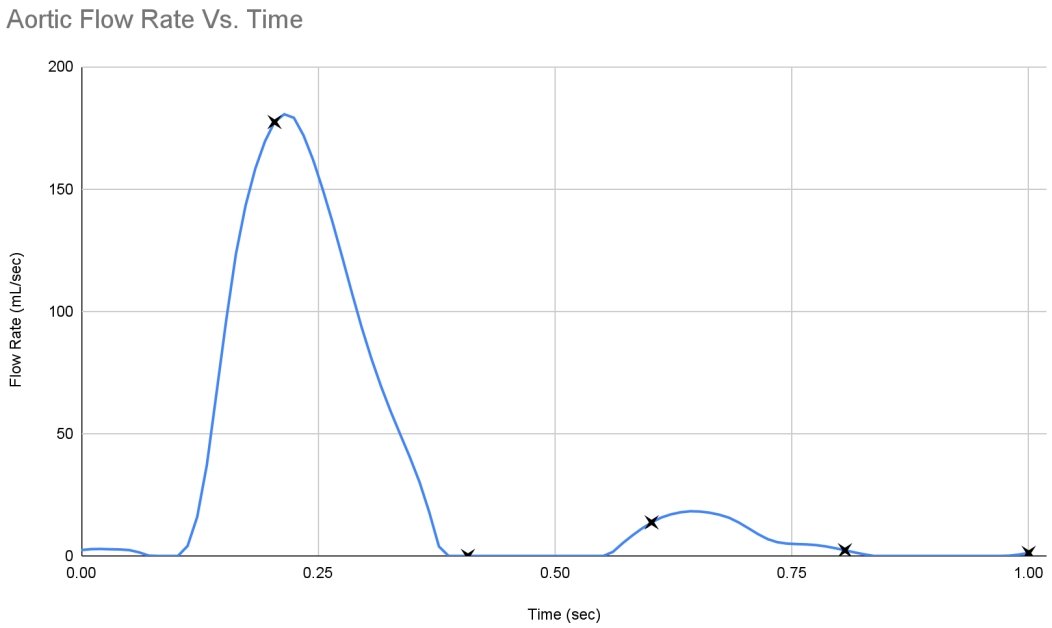

Figure 5: One complete cycle of aortic blood flow in 1 second. The star symbols (✦) represent the 5 flow rates used for flow simulations

Initially, the five aortic flow rates were converted to aortic velocities. Using Equation 3 and the aortic velocities, the corresponding velocities of water were calculated. Finally, water velocity was converted to a flow rate. Table 1 displays the 5 aortic blood flow rates and the dynamically similar water flow rates.

Aortic Blood Flow Rate (mL/min)	Water Flow Rate (mL/min)
10643.13	2660.78
0	0
822.92	205.73
138.30	34.58
73.63	18.41

Table 1: Aortic blood flow rates and dynamically similar water flow rates

3.6 Matching Womersley Number

The Womersley number was used to find the frequency of water that was dynamically similar to hemodynamic conditions. The frequency of water determined how often each water flow rate was programmed to pass through the 3D-printed model.

$$\mu_{water} = 1 * 10^{-3} Pa * s$$
$$\omega_{blood} = 1.33\ cycles/sec$$
$$\rho_{blood} = 1060\ kg/m^3$$
$$\mu_{blood} = 4 * 10^{-3} Pa * sec$$
$$\rho_{water} = 998.21 \frac{kg}{m^3}$$

$$Wo = D * \sqrt{\frac{\omega_{blood} * \rho_{blood}}{\mu_{blood}}} = D * \sqrt{\frac{\omega_{water} * \rho_{water}}{\mu_{water}}}$$

$$\omega_{water} = \frac{\mu_{water} * \omega_{blood} * \rho_{blood}}{\mu_{blood} * \rho_{water}}$$

$$\omega_{water} = \frac{(1*10^{-3} Pa*sec)(1.33 \frac{cycles}{s})(1060 \frac{kg}{m^3})}{(4*10^{-3} Pa*sec)(998.21 \frac{kg}{m^3})} = 0.35 \frac{cycles}{sec}$$

$$\frac{1}{0.35 \frac{cycles}{sec}} = 2.83\ seconds\ for\ a\ full\ cycle$$

Since it should take about 2.83 seconds total for all of the 5 flow rates to be activated, a wait time between each flow rate of 0.57 seconds was added to the program that controlled the pump.

4. Steady Flow Calibrations

4.1 Calibration - L/S Gear Pump

An L/S gear pump from MasterFlex was used for the initial stages of the study which involved trials with steady flow. Calibrations are needed before trials begin to make sure the flow rates outputted were the flow rates calculated according to dynamic similarity. To calibrate the pump, the pump's flow settings were compared to the actual output flows of the pump. 40 total measurements were performed to calculate the actual flow rate of the pump at varying settings. The measurements started with a 100 mL/min flow setting and increased by 100 mL/min until 1000 mL/min was reached. Each increment of 100 mL/min was performed 4 times. At each flow setting, a beaker of 500 mL was filled and the time it took for the beaker to be filled up was recorded. This allowed for the actual flow rate measured at each increment to be compared to the setting of the pump resulting in the following linear equation:

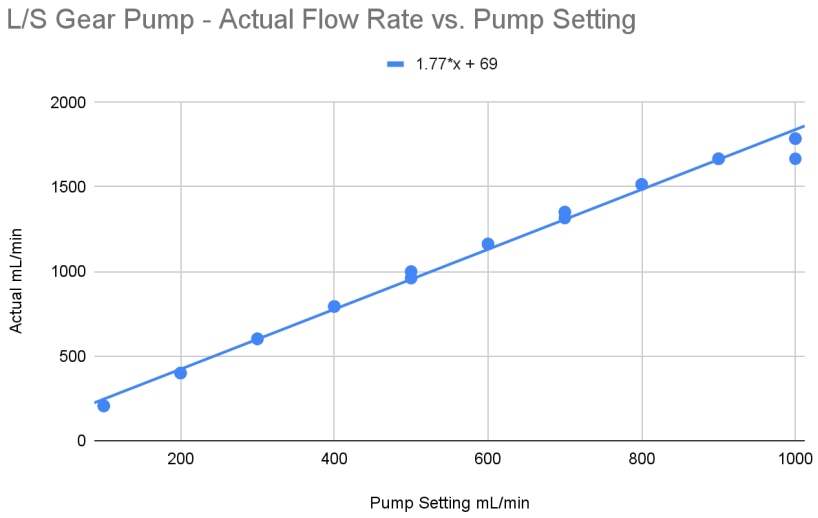

Figure 6 - Actual flow rate vs. pump setting for the L/S pump

(1.77 * Pump Setting $\frac{mL}{min}$) + 69 $\frac{mL}{min}$ = Actual Flow Rate **(4)**

The pump settings did not match the actual flow rate that was outputted because a different pump head from the default was used. Figure 5 shows the actual flow rates calculated and plotted against the pump settings.

Using Equation 4, the corrected flow rate of water was calculated.

$$PumpSetting = \frac{Actual\ Flow\ Rate - 69}{1.77}$$
$$PumpSetting = \frac{1328.89 - 69}{1.77}$$
$$PumpSetting = 711.8\ mL/min \approx 712\ mL/min$$

5. Pulsatile Flow Calibrations and Set Up

5.1 Calibration - Voltage Output and Pressure Values

A multimeter and a 9V power jack were utilized to calibrate the pressure transducer and establish a relationship between voltage and pressure in mmHg. Static pressure calculations were performed to measure the varying voltage outputs of the transducer. Static pressure changes as Δh, the total height of the water, changes. Therefore, tubes filled with water were placed next to each other and attached to the wall. The setup can be seen in Figure 7 to the left. Water was removed from the longer tube on the left until Δh was 0. With each Δh, static pressure was calculated, and the voltage signals of the pressure transducer were recorded. A measuring tape was placed next to the tubes to measure Δh. The bottom ends of both tubes were sealed to the transducer connectors.

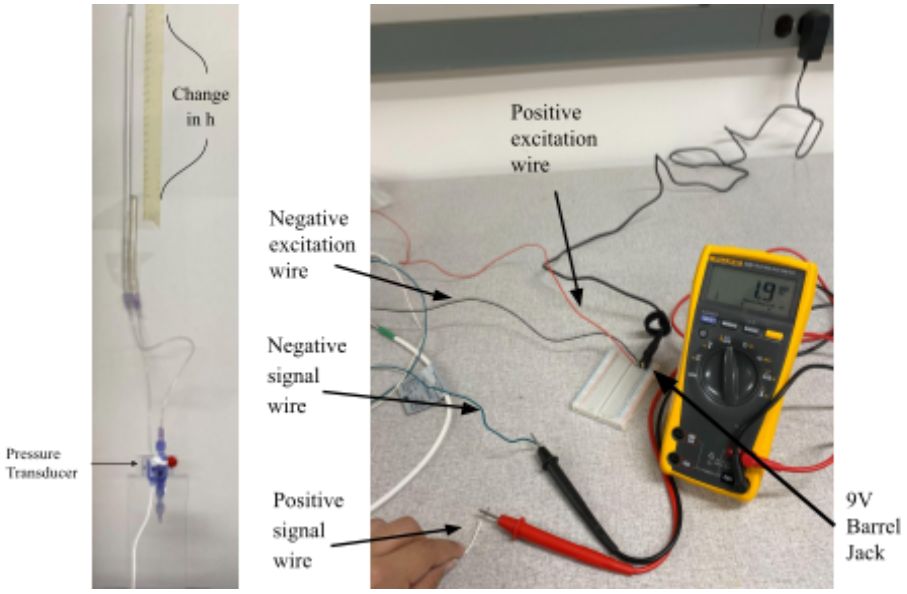

Figure 7 - Setup for pressure transducer calibration

The right side of Figure 7 displays the setup used to read the signal that was returned from the pressure transducer. The positive and negative excitation wires of the transducer were connected to the 9V barrel jack for power. The positive and negative signal wires made contact with the multimeter to display the returning voltage signals in mV.

As the water was removed from the left tube 10 - 60 centimeters at a time, Δh went from about 0.5 m to 0 m. At each varying Δh, the static pressure was calculated, and voltage values were measured. Once Δh reached 0, the left tube was filled with water again for additional trials. Figure 8 displays the relationships between the pressure in mmHg and voltage in mV. The average of the three trials resulted in the following equation:

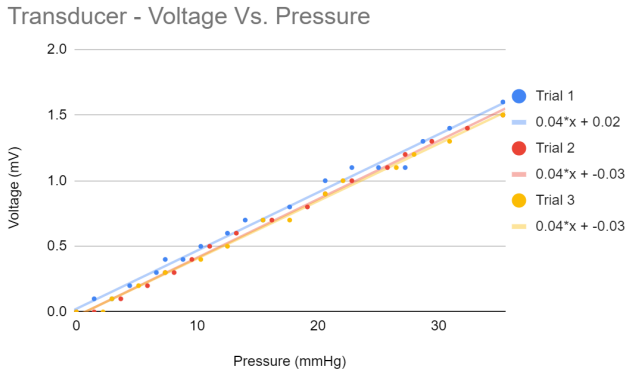

Figure 8- Voltage vs. pressure for pressure transducer

$$0.04\frac{mV}{mmHg} * (Pressure\ mmHg) - 0.01\ mV = Voltage \quad \textbf{(5)}$$

5.2 Calibration - MCP Gear Pump

An MCP ear pump from MasterFlex was used for the pulsatile flow section of the study since this pump has an analog interface through which the pump can be programmed. Two calibrations were needed for this pump because flows less than 2000 mL/min had a different slope and y-intercept than flows greater than 250 mL/min. Having two equations that represent the different ranges of flows made flow rate calibrations more accurate. To calibrate the pump for flow rates greater than 2000 mL/min, three main sections of trials were performed. Each main section had 28 flows tested. The flows started at 2000 mL/min and increased by 100 or 200 mL/min until 3000 mL/min was reached with each increment tested 4 times. At each flow setting, a beaker of 500 mL was filled and the time it took for the beaker to be filled up was recorded. This allowed for the actual flow rate of each trial to be compared to the setting of the pump. Figure 9 displays the results and the final equation that takes the average of the 3 trials is the following:

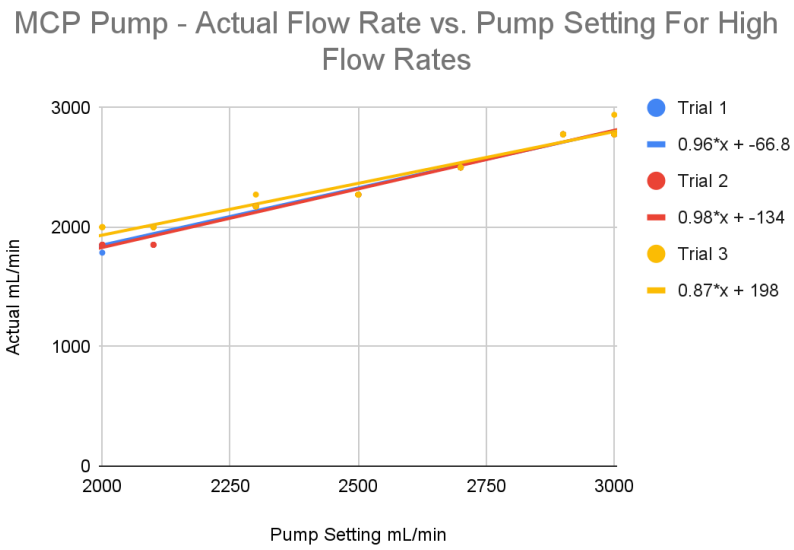

Figure 9 - Actual flow rates vs. pump setting for MCP pump (flow rates above 2000 mL/min)

$$0.94 * (Pump\ Setting\ \frac{mL}{min}) - 0.93\ \frac{mL}{min} = Actual\ Flow\ Rate \quad \textbf{(6)}$$

The calibration done for flows that were lower than 250 mL/min was similar to that of flow rates higher than 2000 mL/min. There were three main trials. Each main section tested 36 flows. The flows started at 40.15 mL/min since this was the closest setting to 40 mL/min and increased by about 20 mL/min until 200 mL/min. Each increment was performed 4 times. For each flow setting, a beaker of 500 mL was filled and the time it took for the beaker to be filled up was recorded. This allowed for the actual flow rate of each test to be compared to the setting of the pump. The results are shown in Figure 10. The average equation from the three trials is shown below:

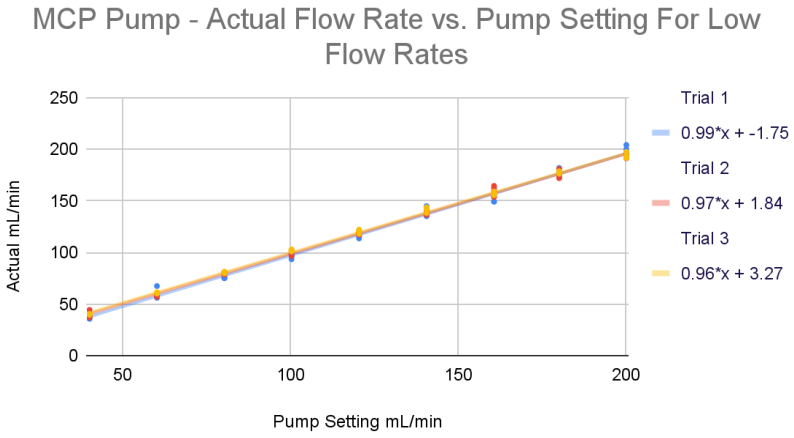

Figure 10 - Actual flow rates vs. pump setting for MCP pump (flow rates below 250 mL/min)

$$0.97 * (Pump\ Setting\ \frac{mL}{min}) + 1.12\frac{mL}{min} = Actual\ Flow\ Rate \quad \textbf{(7)}$$

Using Equations 6 and 7, the corrected water flow rates based on the calibration for the MCP pump can be calculated. Table 2 displays the corrected flow rates of water.

Water Flow Rate (mL/min)	Corrected Water Flow Rate (mL/min)
2660.78	2843.71
0	0
205.73	201.3
34.58	34.77
18.41	19.03

Table 2: Water flow rates for the pulsatile flow study and the corrected water flow rates based on Equations 6 and 7

In addition to the calibration of the pump's regular interface, calibrations were done for the flow output through the analog interface. The pump needed to be remotely controlled to change to the varying flow rates with wait times that match hemodynamic conditions. Calibrations were done to compare the voltage signal received by the analog interface of the pump and the flow rate produced.

The setup for this calibration included a DC power supply that could output different voltage values. While the pump is turned on with power from the wall, the power supply was connected to pins 1, 2, 3, and 5 of the analog connections. An image of the connections can be seen in Figure 11.

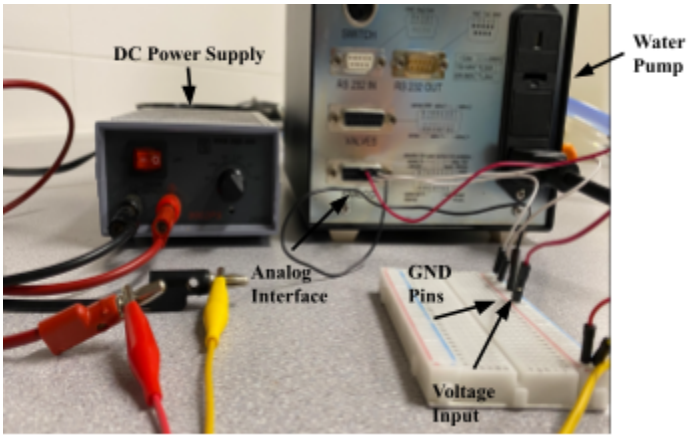

Figure 11 - Setup for calibration of analog control

For this calibration, the voltage settings of 1.5V, 3V, 4.5V, 6V, 7.5V, and 9V were tested 10 times each. As each voltage signal activated the pump, a beaker of 500 mL was filled and the time it took for the beaker to be filled was recorded. The resulting flow rates were averaged for each voltage setting and plotted against the voltage values. The resulting relationship is shown in Figure 12. The final equation was:

$$373 * (VoltageSetting) + 22.4 = Water\ Flow\ Rate \quad \textbf{(8)}$$

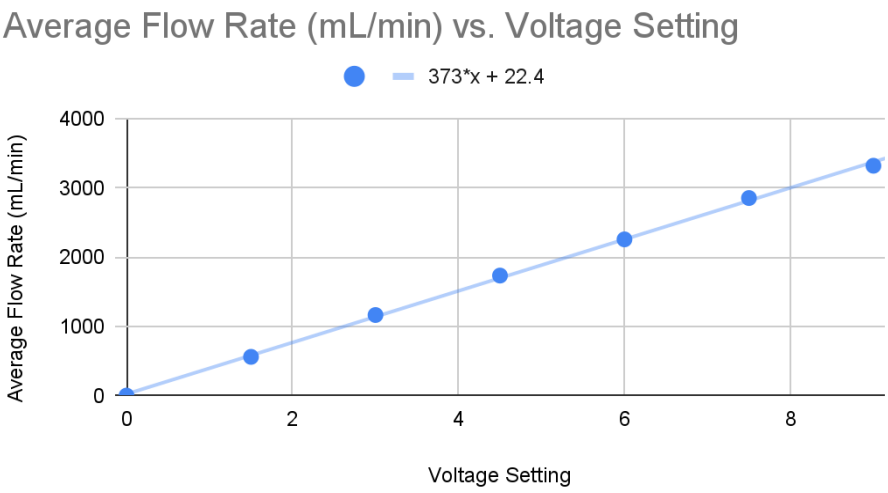

Figure 12 - Average flow rate vs. voltage setting for the MCP pump

Using Equation 8 and the corrected water flow rates, the voltages that needed to be imputed into the analog interface of the pump were calculated. Table 3 displays the results.

Water Flow Rate (mL/min)	Voltage Input (V)
2796.13	7.6
0	0
201.3	0.5
34.77	0.03
19.03	0

Table 3: Corrected water flow rates and their corresponding voltage based on Equation 8

5.3 Analog Control- LabView VI and Setup

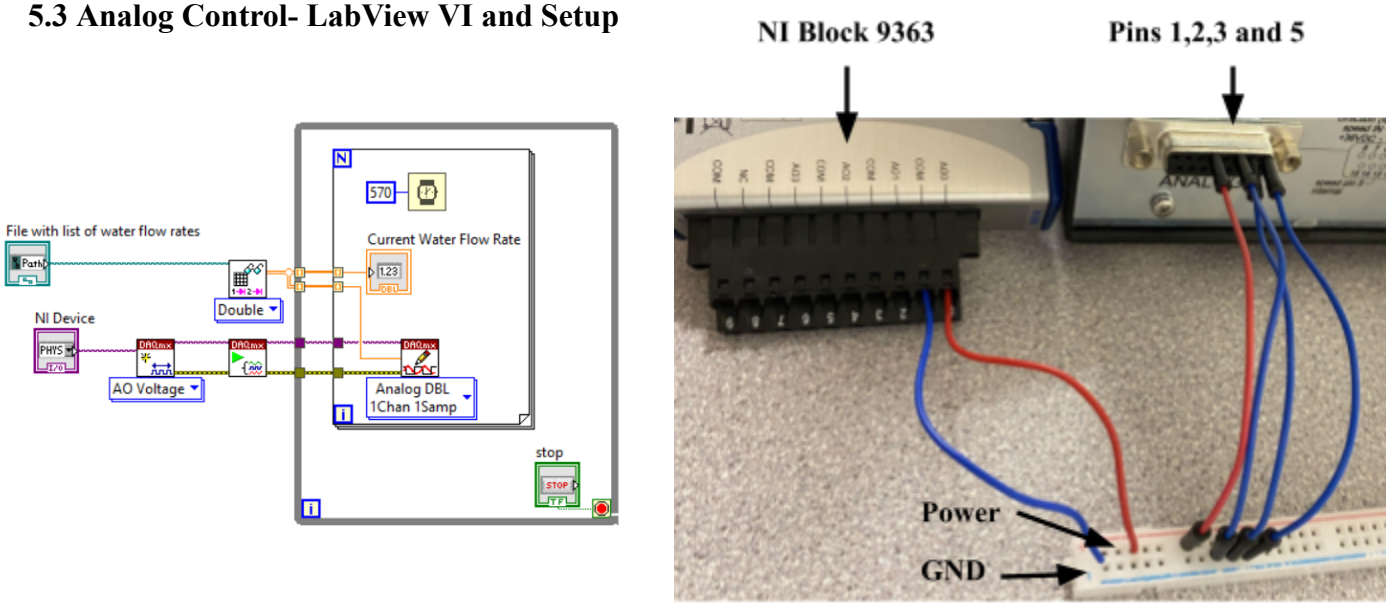

Figure 13 - LabView VI for remote control of MCP pump and electrical setup for trials with pulsatile flow

The pulsatile flow trials were done repeatedly using a LabView VI. The code ran through the voltages listed in Table 3 with a wait time of 0.57 seconds. These voltage values were the output of an NI 9263 Block as analog voltage signals. The setup can be seen in Figure 13. The entrance length remained the same as with the steady flow setup because the parameters for Equation 2 do not change with pulsatile flow.

6. Results and Discussion

6.1 Results of Trials with Steady Flow

As discussed previously, the steady flow for the initial part of the study was set to 712.54 mL/min in accordance with dynamic similarity. A total of 20 trials were executed. Each trial involved running the pump while the pressure transducer measured voltage from the excitation signal produced as a result of the pressure gradient across the occlusion of the 3D-printed model. The average change in voltage measured throughout the 20 trials was 1.42 mV with a standard deviation of 0.08 mV. Using Equation 5 and the average voltage from all 20 trials, the

corresponding pressure gradient produced by the aortic valve occlusion was found. With the use of dynamic similarity, the pressure recovery coefficient is used below to convert the change in pressure of water to the change of pressure of blood.

Finding $\Delta Pwater$

$Voltage = (0.04(\Delta Pwater)) + 0.01$ **(5)**

$\frac{Voltage - y\ intercept\ voltage}{0.04} = \Delta Pwater$

$\frac{1.42\ mV}{0.04}$

$\Delta Pwater = 32.27\ mmHg$

The y-intercept is 0 mV in this case because the starting voltage was subtracted from the final reading of each trial.

Going from $\Delta Pwater \rightarrow \Delta Pblood$

$C_p = \frac{\Delta Pwater}{0.5*\rho water*Vwater^2} = \frac{\Delta Pblood}{0.5*\rho blood*Vblood^2}$

$\Delta Pblood = \frac{\Delta Pwater*\rho blood*Vblood^2}{\rho water*Vwater^2}$

$\Delta Pblood = \frac{32.27 mmHg*1060\ \frac{kg}{m^3}*(0.27\ m/s)^2}{998.21\ \frac{kg}{m^3}*(0.07 m/s)^2}$

$\Delta Pblood = 484.21\ mmHg$

Standard Deviation

The standard deviation for all 20 trails was calculated to be 0.08 mV. In the calculations below, ±0.08 mV were added/subtracted from the average voltage reading, and the resulting pressure gradients were computed. A maximum error of ± 32 mmHg was calculated.

Adding the standard deviation to Avg. voltage

$1.42\ mV + 0.08\ mV = 1.5\ mV$

Finding the resulting pressure gradient for water

$\frac{Voltage - y\ intercept\ voltage}{0.04} = \Delta Pwater$

$\frac{1.5\ mV}{0.04} = 34.09\ mmHg$

Converting from ΔP_{water} to ΔP_{blood}

$\Delta Pblood = \frac{34.09\ mmHg*1060\ \frac{kg}{m^3}*(0.27\ m/s)^2}{998.21\ \frac{kg}{m^3}*(0.07 m/s)^2}$

$\Delta Pblood = 511.49\ mmHg$

Subtracting the standard deviation to Avg. voltage

$1.42\ mV - 0.08 mV = 1.34\ mV$

Finding the resulting pressure gradient for water

$\frac{Voltage - y\ intercept\ voltage}{0.04} = \Delta Pwater$

$\frac{1.34\ mV - 0\ mV}{0.04} = 30.455\ mmHg$

Converting from ΔP_{water} to ΔP_{blood}

$\Delta Pblood = \frac{34.46\ mmHg*1060\ \frac{kg}{m^3}*(0.27\ m/s)^2}{998.21\ \frac{kg}{m^3}*(0.07 m/s)^2}$

$\Delta Pblood = 451.475\ mmHg$

6.2 Steady Flow Discussion

A pressure drop of 484.21 mmHg is unrealistically high for patients with aortic stenosis (Hoeijmakers et al., 2019). The steady flow trials are not an accurate representation of hemodynamic conditions since blood flow is highly unstable. This likely impacted the final pressure readings since unsteady flow structures appear in pulsatile flow that are not present in steady flow. With pulsatile flow, the velocity of the flow changes as it passes through the aortic valve; steady flow is unable to mimic the irregularity of blood velocity over time. Additionally, vortices form with irregularity when the flow is unsteady which was not taken into account in the trials with steady flow. Vortices change as the flow travels and predicting their size and strength is nearly impossible with flow models. The presence of vortex shedding, vortex roll-up, vortex pairing, vortex sheet breakup, as well as other structures happen only with pulsatile flow. Therefore, it is reasonable that the results did not reflect a realistic pressure gradient. Nevertheless, since the resulting pressure was not extremely far from a realistic pressure drop across the valve for severe aortic stenosis, more testing with the pulsatile flow was performed. The results are referenced below.

6.3 Results of Trials with Pulsatile Flow

For the pulsatile flow trials, the flow was programmed to go through a cycle of 5 flows, representing 5 evenly spaced points of the flow of blood through the aortic valve. As discussed previously, flow rates were chosen using aortic flow data, displayed in Figure 5, and converted to water flow rates with the use of Equation 3. Equations 6 and 7 were then used to correct the water flow rates based on calibrations done for the pump. Some of these points were extremely low and others were negative due to the backflow of blood which allowed the code to have 3 real flows the pump could deliver. The remaining two flows were set equal to 0. The highest flow rate represents the peak velocity reached during systole as the heart pumps blood out. The second-highest peak represents the flow rate of blood when the aorta contracts. Lastly, the corrected flow rates were translated to the necessary voltage inputs using Equation 8. The voltages were sent to the pump's analog interface using a 9263 NI block with a wait of 0.57 seconds between each flow to be consistent with real blood flow. The sequence of voltages was tested 9 times for each trial and there were 4 trials in total. The resulting average pressure gradients are displayed in Table 4.

Voltage (V)	Avg. Pressure Change (mmHg)	Standard Deviation (mmHg)
7.6	304.19	9.1
0	0	0
0.5	34.08	0
0.03	0	0
0	0	0
Average	112.97	

Table 4 - Pressure gradient results with pulsatile flow

6.4 Pulsatile Flow Discussion

The results shown in Table 4 have a range of about 0 mmHg - 305 mmHg with a standard deviation between 0 mmHg and 9.1 mmHg. There is a standard deviation of zero for the majority of the points because the flow is very low at most parts of the cycle ranging from 0 mL/min to 201 mL/min. These low flow rates do not cause a significant change in pressure. For the peak flow rate, pressure gradient values increase rapidly which leads to more discrepancies in readings.

Nonetheless, these results are much closer to the real pressure gradient experienced by patients with aortic stenosis in comparison to the results of the steady flow trials. The changes in pressure gradients with different voltage inputs are promising since they provide more information than that of a single flow rate value. Therefore, the results prove that programmed pulsatile flow simulations can represent what happens in the human body more accurately than steady flow trials. Additionally, sources of error could be identified and corrected so that the overall model becomes more accurate and useful to health professionals.

Moreover, severe aortic stenosis could be diagnosed for this patient given the extremely high pressure gradient of 304.19 mmHg measured across the aorta during peak velocity. This patient is in danger of serious side effects such as heart failure, atrial fibrillation, and syncope. Since such symptoms can result in a life expectancy of 4 years at most, a valve replacement could be the only treatment option (Delong & Sharma, n.d.). Deciding on a final treatment depends on the patient's ability to undergo surgery as well as medical history regarding other heart diseases or symptoms experienced. The procedure followed in this study could serve as one of the primary forms of measuring the pressure drop across the aorta since it takes into account patient-specific calcification. If hemodynamic conditions were modeled more accurately, using more flow rate points and with a more advanced data acquisition method, this is an optimistic experiment.

6.5 Sources of Error Discussion

Leaks are a usual problem in flow simulations that use liquids as the main fluid. In this study, silicone glue, tube adapters, and tubing clamps were used to avoid significant leaking. Though not major, some leaking was still present in the experiments which could have led to some errors in terms of pressure gradients. Bubbles and impurities are also common issues when utilizing water. When present, these disrupt the flow and could lead to incorrect readings from the pressure transducer.

The data gathered for both simulations was based on multimeter readings captured either through video or live in person. This could lead to various errors as the multimeter captured voltage values with an accuracy of 0.01 mV. The difference between 0.01 mV and 0.02 mV in blood pressure is about 3.5 mmHg. More mistakes could have also taken place when reading voltage values manually without the use of a data collection interface. With the pulsatile flow trials, voltage values changed within 0.57 seconds so there could be human error in the recording

of results. These things combined could have caused an overestimation or underestimation of pressure gradient values across the aorta.

The electrical setup and equipment used could have had errors when operating. It is known that a connection that is not secured properly could lead to a change in the signal received due to loss of contact. Electrical noise could have also led to incorrect readings in voltage. Additionally, the pumps and pressure transducers used could have outputted incorrect flows or readings. Errors in calibration procedures could have also led to incorrect output flows, voltage readings, or voltage outputs.

Segmentation of CT scan images could have led to errors in the main geometry of the 3D-printed model. Manual segmentation depends on the ability to differentiate between tissue, blood, and calcium buildup. Such can be difficult because CT scan images are limited in resolution which could lead to a misinterpretation of what each region in the image represents. Additionally, the 3D printed model used was made using rigid plastic instead of a material that mimics the flexible characteristics of real tissue. The misrepresentation of the aortic valve could have further led to incorrect results.

6.6 Future Work

Further work with the pulsatile flow simulation would be beneficial as this was the most accurate part of the study. One improvement would be incorporating equipment for data acquisition. This would decrease the possibility of human error when interpreting results. Another key advancement would be using varying 3D printed models from different patients with varying severity of calcification. This would reveal if this patient-specific procedure works better for a certain level of aortic stenosis severity. Nevertheless, this would require more information from a medical institution such as Tufts Medical Center and specific details about the patient's diagnosis. Such use of patient data might require IRB approval.

Varying materials of 3D printing filament could be tested as well. There could be a correlation between the material of the 3D-printed model and the accuracy of the results. Furthermore, since plastic is very rigid, it is unable to serve as a good imitation of human tissue. Future experiments could use a material that is more flexible to mimic the aortic valve better. They could also implement artificial valves used for surgical replacements to study which type is the most beneficial for patients. In addition to a change in material, more flow rate points could be extracted from Figure 5 for a more accurate flow cycle.

7. Acknowledgments

Thank you to Assistant Teaching Professor, Dr. Erica Kemmerling, for her continuous guidance, help, and advocacy during the entire study. Thank you to the resident Cardiologist at Tufts Medical Center, Dr. Luis Gonzales, who provided the CT scan images that made this study possible. Thank you to Tufts Facilities, Bray Lab Staff, Associate Professor, Robert White, and Part-time Lecturer, Brandon Stafford, for their help with the electrical setup. Thank you to the research committee for being a part of this process. Thank you to the Mechanical Engineering

Department at Tufts for allowing this study to take place in the Tufts Body Flow Laboratory in the Bray Lab building as well as access to the 3D Printing Laboratory of Bray Lab.

References

Aortic stenosis. (2022, January 9). MedlinePlus. Retrieved April 20, 2023, from https://medlineplus.gov/ency/article/000178.htm

Carabello, B. A., & Paulus, W. J. (2009, March 14). Aortic stenosis. *The Lancet*, *373*(9667), 956-966. 10.1016/S0140- 6736(09)60211-7

Cardiac Imaging: Types, Uses and Procedure Details. (2022, May 3). Cleveland Clinic. Retrieved April 20, 2023, from https://my.clevelandclinic.org/health/diagnostics/16836-cardiac-imaging

Clark, C. (1976). Turbulent velocity measurements in a model of aortic stenosis. *Journal of Biomechanics*, *9*(11), 677-687. https://doi.org/10.1016/0021-9290(76)90169-X

Delong, C., & Sharma, S. (n.d.). *Physiology, Peripheral Vascular Resistance - StatPearls*. NCBI. Retrieved April 20, 2023, from https://www.ncbi.nlm.nih.gov/books/NBK538308/

Ghalichi, F., Deng, X., Champlain, A. D., Douville, Y., King, M., & Guidoin, R. (1998). Low Reynolds number turbulence modeling of blood flow in arterial stenoses. *Biorheology*, *35*(4-5), 281-294.

Garcia, J., van der Palen, R., Bollache, E., Jarvis, K., Rose, M. J., Barker, A. J., Collins, J. D., Carr, J. C., Robinson, J., Rigsby, C. K., & Markl, M. (2018). Distribution of blood flow velocity in the normal aorta: Effect of age and gender. Journal of magnetic resonance imaging: JMRI, 47(2), 487–498. https://doi.org/10.1002/jmri.25773.

Grimard, B. H., Safford, R. E., & Burns, E. L. (2016). Aortic Stenosis: Diagnosis and Treatment. American family physician, 93(5), 371–378.

Hatle, L., Angelsen, B. A., & Tromsdal, A. (1980, March 1). Non-invasive assessment of aortic stenosis by Doppler ultrasound. *Heart*, *43*(3), 284-292.

Hayek, A., Derimay, F., Green, L., Rosset, M., Thibault, H., Rioufol, G., & Finet, G. (2020, August 29). Impact of Arterial Blood Pressure on Ultrasound Hemodynamic Assessment of Aortic Valve Stenosis Severity. Journal of the American Society of Echocardiography, 33(11), 1324-1333. https://doi.org/10.1016/j.echo.2020.06.013

Heart failure - Symptoms and causes. (2023, March 11). Mayo Clinic. Retrieved April 20, 2023, from https://www.mayoclinic.org/diseases-conditions/heart-failure/symptoms-causes/syc-20373142

Hoeijmakers, M.J.M.M., Soto, D.A.S., Waechter-Stehle, I., Kasztelnik, M., Weese, J., Hose, D.R., & Van De Vosse, F. N. (2019, 9). Estimation of valvular resistance of segmented aortic valves using computational fluid dynamics. *Journal of Biomechanics*, *94*, 49-58. https://doi.org/10.1016/j.jbiomech.2019.07.010

Keshavarz-Motamed, Z., & Kadem, L. (2011, April). 3D pulsatile flow in a curved tube with coexisting model of aortic stenosis and coarctation of the aorta. *Medical Engineering & Physics*, *33*(3), 315-324. https://doi.org/10.1016/j.medengphy.2010.10.017

Loudon, C. (1998). The Use of the Dimensionless Womersley Number to Characterize the Unsteady Nature of Internal Flow. Theoretical Biology, 63-78. https://www.academia.edu/27228277/The_Use_of_the_Dimensionless_Womersley_Number_to_Characterize_the_Unsteady_Nature_of_Internal_Flow

Maragiannis, D., Jackson, M. S., Igo, S. R., Chang, S. M., Zoghbi, W. A., & Little, S. H. (2014, September). Functional 3D Printed Patient-Specific Modeling of Severe Aortic Stenosis. *Journal of the American College of Cardiology*, *64*(1066–1068). https://doi.org/10.1016/j.jacc.2014.05.058

Morini, G. L. (n.d.). Entrance Region. *Encyclopedia of Microfluidics and Nanofluidics*, 621–630. https://doi.org/10.1007/978-0-387-48998-8_485

Namasivayam, M., He, W., Churchill, C. W., Capoulade, R., Liu, S., Lee, H., Danik, J. S., Picard, M. H., Pibarot, P., Levine, R. A., & Hung, J. (2020, April 21). Transvalvular Flow Rate Determines Prognostic Value of Aortic Valve Area in Aortic Stenosis. *Journal of the American College of Cardiology*, *75*(15), 1758-1769. https://doi.org/10.1016/j.jacc.2020.02.046.

National Library of Medicine. MedlinePlus (n.d.). Retrieved April 26, 2023, from https://vsearch.nlm.nih.gov/vivisimo/cgi-bin/query-meta?v%3Aproject=medlineplus&v%3Asources=medlineplus-bundle&query=angina

Padmanabhan, N. (1980, May). Mathematical model of arterial stenosis. *Medical & Biological Engineering & Computing*, *18*, 281–286. https://doi.org/10.1007/BF02443380

Syncope (Fainting). (2022, November 16). American Heart Association. Retrieved April 27, 2023, from https://www.heart.org/en/health-topics/arrhythmia/symptoms-diagnosis--monitoring-of-arrhythmia/syncope-fainting

The Texas Heart Institute. (n.d.). Diastolic Dysfunction. TexasHeart. Retrieved April 26, 2023, from https://www.texasheart.org/heart-health/heart-information-center/topics/diastolic-dysfunction/

Voelker, W., Reul, H., Ing, G. N., Ing, T. S., Ing, B. S., Ing, A. A. S., & Karsch, K. R. (1995, February 15). Comparison of Valvular Resistance, Stroke Work Loss, and Gorlin Valve Area for Quantification of Aortic Stenosis. Journal of the American Heart Association, 91.

Voelker, W., Reul, H., Stelzer, T., Schmidt, A., & Karsch, K. R. (1992, December). Pressure recovery in aortic stenosis: An in vitro study in a pulsatile flow model. *Journal of the American College of Cardiology*, *20*(7), 1585-1593. Journal of the American College of Cardiology